Self-Referenced Single-Electron Quantized Current Source

Lukas Fricke,[†] Michael Wulf,[*] Bernd Kaestner, Frank Hohls,[‡] Philipp Mirovsky, Brigitte Mackrodt, Ralf Dolata, Thomas Weimann, Klaus Pierz, Uwe Siegner, and Hans W. Schumacher
Physikalisch-Technische Bundesanstalt, Bundesallee 100, 38116 Braunschweig, Germany
(Received 24 January 2014; published 6 June 2014)

The future redefinition of the international system of units in terms of natural constants requires a robust, high-precision quantum standard for the electrical base unit ampere. However, the reliability of any single-electron current source generating a nominally quantized output current $I = ef$ by delivering single electrons with charge e at a frequency f is eventually limited by the stochastic nature of the underlying quantum mechanical tunneling process. We experimentally explore a path to overcome this fundamental limitation by serially connecting clocked single-electron emitters with multiple *in situ* single-electron detectors. Correlation analysis of the detector signatures during current generation reveals erroneous pumping events and enables us to determine the deviation of the output current from the nominal quantized value ef. This demonstrates the concept of a self-referenced single-electron source for electrical quantum metrology.

DOI: 10.1103/PhysRevLett.112.226803 PACS numbers: 73.23.Hk, 06.20.−f, 85.35.Gv

Quantum metrology promises measurement standards providing highest precision and universality by making reference to fundamental constants [1]. In electrical quantum metrology two macroscopic quantum effects—the Josephson effect [2] and the quantum Hall effect [3]—have enabled versatile quantum standards for the units volt and ohm, respectively. The anticipated redefinition of the international system of units (SI) based on quantum metrology, however, requires a quantum standard for the SI base unit ampere [4,5]. Many candidates for such quantum current standard such as single electron pumps have been explored [6–16]. Among them dynamic semiconductor quantum dots (QDs) [13–15] have recently demonstrated promising characteristics. Such devices do not rely on a robust macroscopic quantum effect, but on quantum mechanical tunneling during the periodic capture and release of a single charge e [17–21]. However, the stochastic nature of tunneling inevitably leads to small random deviations from the ideally quantized current of $I = ef$, with f the pumping rate, hindering the realization of a robust quantum current source with lowest uncertainty.

As an alternative approach the counting of electrons passing randomly through a nanostructure has been explored [22,23]. However, the sensitivity and bandwidth of single-charge detectors place severe limits on the current amplitude and achievable uncertainty. The late M. Wulf proposed [24] a way to overcome these fundamental problems of quantum-current metrology by combining single-electron pumping and single-electron detection in one device: the self-referenced single-electron current source. Here a nominally quantized single-electron current is generated in a serial arrangement of single-electron pumps and single-electron detectors [25]. During self-referenced operation only rare stochastic pumping errors are detected to determine the deviations from the nominal current $I = ef$ allowing the realization of a low-uncertainty single-electron quantum current source with validated output current. However, such self-referenced current generation has not been experimentally demonstrated yet.

Here, we present a quantum circuit integrating QD single-electron pumps and single-charge detectors to implement a self-referenced single-electron current source at low frequencies. Statistical analysis of the error detection yields the corrected output current with the current uncertainty reduced by more than one order of magnitude as compared to an individual single-electron pump. In principle, the device allows scaling to higher currents and lower

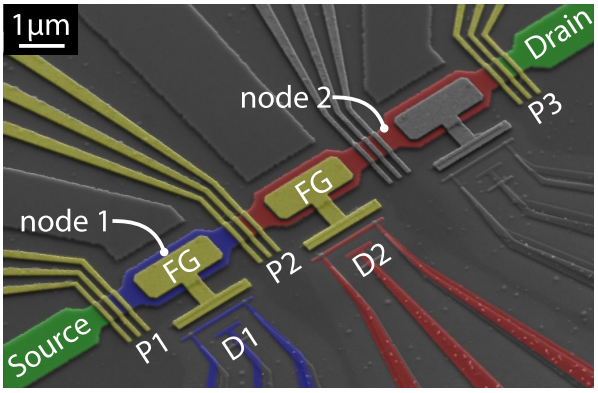

FIG. 1 (color online). SEM image of the device. The semiconductor part between source and drain (green) consists of three pumps $P1$-$P3$ and two charge nodes 1,2 (blue, red). Each pump is defined by three metallic top gates (yellow) forming a QD in the semiconductor. Between $P2$ and $P3$, another pump (gray) is not used and grounded. The charge detectors $D1$ (blue) and $D2$ (red) are coupled to the nodes via floating gates (FG, yellow).

uncertainties for use as a robust and validated quantized-current standard for the SI base unit ampere.

The device is a hybrid semiconducting-metallic nanostructure as shown in Fig. 1 [20]. From the lower left to the upper right a semiconducting channel is formed by etching a GaAs/AlGaAs heterostructure with a high-mobility two-dimensional electron gas (2DEG) situated 90 nm underneath the surface. The 2DEG channel consists of source and drain (green) and intermediate nodes 1,2 (blue, red) each separated by one of the three single-electron pumps $P1$-$P3$. Each pump is defined by three metallic top gates (yellow) crossing the channel. The electrical potentials of the nodes and hence the nodes' charge states are monitored by two single-electron transistors (SET) [26,27] operated as charge detectors $D1$ (blue) and $D2$ (red), respectively. The SETs are fabricated by two-angle shadow evaporation of aluminium [28]. For enhanced capacitive coupling to the nodes, gates with floating potentials (FG, yellow) are deposited. The SET detectors are operated at fixed bias voltage. The current, acting as detector signal, is measured by synchronized digitizer cards at a sampling rate of 12 kS/s after digital averaging. Doing so we oversample the detector response by about 20 times. The measurements are performed in a dry dilution cryostat at nominal base temperature of about 25 mK.

The principle of the QD pump has been discussed in detail in Refs. [14,19,20,29,30]. The robust serial operation of these pumps has been demonstrated in Ref. [25] and has been adapted as follows: By applying negative voltages of about -200 mV to the first two gates of each pump (entrance and exit gate, respectively) isolated QDs are formed. (The third gate of each pump is grounded.) For these voltages the QD ground state is above the chemical potential of the semiconductor channel and the QD is empty. To induce pumping of a single electron, a single, cosine-shaped pulse with frequency $f = 40$ MHz and amplitude $V = -75$ mV at the output of the generator is superimposed onto the entrance gate of pump i. During the pulse the entrance barrier is first lowered to allow tunneling onto the QD from the source and then raised back up. In this cycle n_i electrons are captured from the pump's source side in the QD with probability $p_n^{(i)}$ and subsequently emitted to the drain side. Note that whenever no pump pulse is applied, the high gate barriers of the QD prevent electrons from tunneling between the nodes.

A sketch of the pulse shape and the pulse sequence during operation is shown in Fig. 2(a). The pulses are delayed by $\tau = 20$ ms each which is about ten times larger than the detector response time $\tau_d \approx 1.5$ ms allowing reliable charge detection. The pulses of the sequence can be separated in two groups. The first three pulses [(i)–(iii)] constitute a marker sequence. Here, we pump $n = 1$ additional electron sequentially through the structure from source to node 1, to node 2, and to drain by subsequent application of a pulse to $P1$, $P2$, and $P3$. This allows

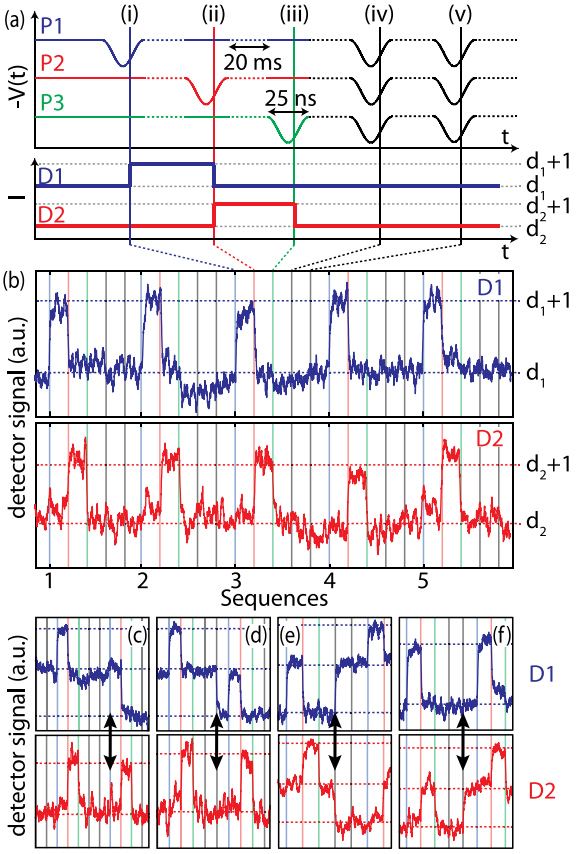

FIG. 2 (color online). Self-referenced current source operation. (a) Sketch of pulse sequences for $P1$, $P2$, and $P3$ with nominal detector signals $D1$, $D2$ for error free pumping of $1e$ per pulse. A marker sequence [pulses (i)–(iii)] shuttles one electron through the structure sequentially. Subsequently, $P1$-$P3$ are triggered twice simultaneously [(iv)–(v)]. Here, only transfer errors are monitored. (b) Corresponding measured signals. Vertical lines indicate pump pulses, horizontal dashed lines mark the charge states $d_{(1,2)}, d_{(1,2)} + 1$ of each node 1, 2. (c)–(f) Signatures of missing-cycle events marked by double arrows: (c) During the marker sequence by pump $P1$, (d)–(f) in series operation by pump $P1$, $P2$, and $P3$, respectively.

calibration of $D1$ and $D2$ in terms of the signature of $n = 1$ (or more) additional electrons on node 1 and 2 (see the Supplemental Material [31]). It further yields the probability $p_n^{(i)}$ of each pump i of pumping n_i electrons per pumping cycle. By the last two pulses (iv)–(v) of the sequence $P1$-$P3$ are triggered simultaneously. Here the detection scheme changes from an absolute measure of number of transferred electrons to the detection of pumping errors as described below.

The expected detector signals $D1$ (blue) and $D2$ (red) during one sequence are sketched at the bottom of Fig. 2(a). Here we assume that all pumps transfer exactly one electron per pulse. Horizontal dashed lines indicate the two detector states $d_{(1,2)}, d_{(1,2)} + 1$ of node (1,2) reflecting a change in the number of electrons on the corresponding node by one electron. When triggering pump $P1$ [pulse (i)], one electron

is transferred from the source lead to node 1, leading to a step in $D1$ while $D2$ remains unaffected. By the following pulse (ii) one electron is transferred across $P2$ from node 1 to node 2, resulting in a step in both detectors with opposite sign. $D1$ returns to the initial value d_1 and $D2$ increases to $d_2 + 1$. Lastly in the marker sequence, pump $P3$ is triggered (iii) removing one electron from node 2 to drain with $D2$ returning to its initial state. In the following synchronized pumping (iv),(v), $D1$ and $D2$ both remain in their initial state as one electron is pumped on and off each node leaving the node charge unchanged. The same behavior is observed in the experimental data of error free pumping in Fig. 2(b). Here the measured signals of $D1$ (blue) and $D2$ (red) are shown during five consecutive pumping sequences (1–5) as described above. The colored vertical lines indicate the different pulses (i)–(v) as marked in Fig. 2(a) (see dashed connection lines). The two charge states $d_{(1,2)}, d_{(1,2)} + 1$ of both nodes and thus the charge transfer are reliably detected.

Also stochastic tunneling errors can be identified and attributed during sequential and synchronous operation as shown in Figs. 2(c)–2(f). During the marker sequence the transferred charges are measured directly. Figure 2(c) shows the detector signals of an event where $P1$ fails to pump an electron during pulse (i) (arrow). $D1$ and $D2$ thus remain in the same state before and after pulse (i). However, by pulse (ii) $P2$ transfers an electron from node 1 to node 2 thereby shifting the baseline of detector $D1$ by $-1e$. Accordingly, errors of $P2$, $P3$ in the marker sequence can be reliably detected and statistically analyzed.

Figures 2(d)–2(f) further show detector traces of error detection during synchronous pumping (iv),(v). In Fig. 2(d) $D1$ shows a drop indicating that the charge of node 1 is reduced by $1e$ while the charge of node 2 remains constant. This signature is most likely the consequence of $P1$ missing to pump an electron while $P2$ and $P3$ are operating properly. If pump $P2$, connecting both nodes, misses a pump cycle, this should result in a simultaneous change of $D1$, $D2$ with opposite sign: the charge of node 1 increases by $1e$, whereas the charge of node 2 is lowered by $1e$. This is marked by the arrow in Fig. 2(e). In case of pump $P3$ missing a cycle, node 1 remains unaffected and only the detector $D2$ detects an additional electron on node 2 as shown in Fig. 2(f).

The data demonstrate the detection of individual pumping errors during synchronous serial pumping. However, the above error signatures can not be unambiguously attributed to failures of the individual pumps $P1$-$P3$. As an example, the signature of perfect series operation with both detectors at constant level could also result from simultaneous failure of all pumps [24]. To illustrate this, we analyze the possible scenarios of Fig. 2(f) in more detail. Figure 3(a) shows the detector signal (left) and a schematic of the node charge (right): $D1$ shows a constant number of electrons (d_1) on node 1 while $D2$ indicates an additional electron ($d_2 + 1$) on node 2. The table below contains three possible scenarios of charge transfer and their corresponding probabilities which are compatible with the observed detector signature. The probability for transferring n electrons across $P3$ is derived from the characterization of the pumping statistics of each pump by analyzing the marker sequence (see the Supplemental Material [31]). As mentioned above, the most likely explanation of this signal is a missing pump event by pump $P3$ (first line). This scenario is the most probable one with probability of 0.9999. But also a simultaneous error by the other two pumps $P1$ and $P2$, both transferring two electrons, results in this signature. Considering the working points of the pumps, this coincidental error of $P1$ and $P2$ is quite unlikely with a probability of 10^{-4} (second line). The next-order process leading to the same charge signals involves erroneous pumping by all three pumps transferring $n_{(1,2,3)} = (3, 3, 2)$ (line 3) and has only a probability of about 10^{-9}. Generally, the probability of an event scales inversely with the number of failing pumps involved. The same argument holds for the introductory example: For the given device and operation parameters the probability of all pumps failing in synchronous operation instead of transferring one electron is 1.5×10^{-5}. Such higher-order processes lead to a slight broadening of the final probability distribution and hence to a small increase of the output current uncertainty.

In contrast Fig. 3(b) shows a signature $(d_1 + 1, d_2)$ which cannot be identified with high reliability as two scenarios are of almost same probability: a coincidental error by $P2$, $P3$ missing the transfer, and an error by $P1$ transferring two electrons with slightly higher probability. In such case the large probability of misattribution leads to an abrupt broadening of the electron number distribution and hence of the uncertainty of the output current.

By statistical analysis of long series of pumping events we obtain the output current and its full uncertainty distribution. The actual current output of the device corresponds to the number of electrons transferred across $P3$ to drain. Figure 3(c) shows two examples of the deviation of the output from the nominal quantized current as a function of pulse index. Each jump in the traces in Fig. 3(c) reflects a deviation of one electron across $P3$: in the green trace in total, nine electrons are missing (2.1%) and in the blue trace seven (1.3%).

Yet, not only the absolute number of transferred electrons is obtained, but also the full probability distribution of the different possible scenarios and hence the full uncertainty of the output current. The statistical analysis of the output current for both traces of Fig. 3(c) are shown in Figs. 3(d)–3(e). The probability distribution in Fig. 3(d) after accounting (green bars) of the green trace has significantly narrowed compared to the probability distribution of pump $P3$ (gray). However, during pumping several detector events with scenarios of comparable

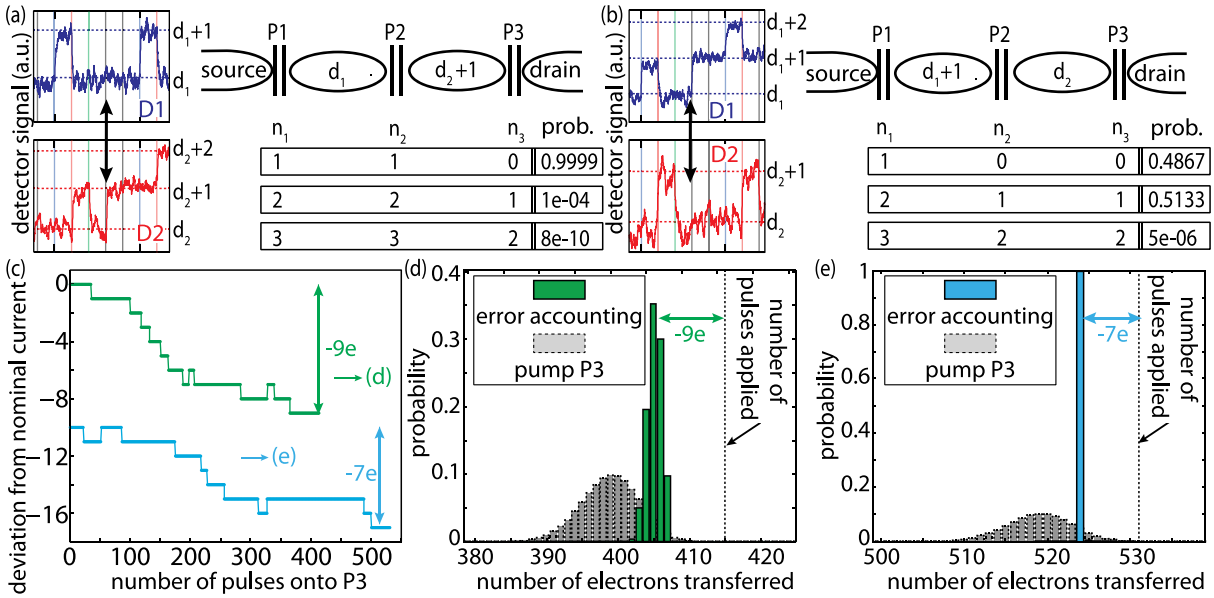

FIG. 3 (color online). Error analysis. (a) Error signature $(d_1, d_2 + 1)$ measured (left) and sketched (right) with different realization scenarios and probability vector. (b) Error signature $(d_1 + 1, d_2)$ measured (left) and sketched (right). (c) Deviation from nominal current across $P3$ versus pulse index for two working points of the pumps. Curves are offset by $-10e$. (d) Probability distribution of the number of pumped electrons of the green (upper) trace in (c) including error accounting (green, solid) and expected distribution of pump $P3$ (gray, dashed lines). The number of pump pulses applied to $P3$ is marked (dashed vertical line). (e) Corresponding plot of probability distributions for the blue (lower) plot in (c) of the individual pump $P3$ (gray) and the self-referenced current source (blue).

probability [cf. Fig. 3(b)] result in a still considerable uncertainty. The expectation value resulting from the distribution is 405.2 ± 1; i.e., we expect after error accounting to transfer 405 electrons. Without accounting (gray distribution), we expect to transfer most likely 399 ± 4.1 electrons with the uncertainty given in both cases by the square root of the variance of the probability distribution.

In contrast, in the data of Fig. 3(e) the working points were chosen such that only distinguishable errors occurred. This results in a very narrow probability distribution after error accounting (blue bars) compared to the distribution for the individual $P3$ (gray bars). After error accounting, we know that 524 electrons have been transferred with a probability of 99.4% by 531 pulses onto $P3$ (electron number uncertainty ± 0.08), whereas for the individual pump $P3$ we expect on average 519 ± 3.9 electrons. The self-referenced output current equals to an average current of $I = 4.743 \times 10^{-18}$ A over 17.7 s with an uncertainty of 0.7×10^{-21} A. Compared to the individual pump $P3$, the uncertainty is reduced by a factor of about 50 and thus by more than one order of magnitude.

In the future, the output uncertainty of a such self referenced single electron pump can be significantly reduced: Tuning the pumps to asymmetric transfer rates makes transfer of more than one electrons very unlikely. Furthermore, the addition of further pumps and detectors in the serial arrangement exponentially reduces the probability of correlated errors.

This work demonstrates a self-referenced current source at a repetition frequency of about 30 Hz, i.e. in the limit $f \ll 1/\tau_d$. Here, we are able to resolve the outcome of each pump pulse. When operated at higher repetition frequencies above the detector bandwidth, error events may be missed, thus leading to potential misattributions. Therefore, the ratio of the average time between errors $((1 - p_1)f)^{-1}$ to the detector bandwidth $1/\tau_d$ has to be included in the statistical analysis then. The remaining uncertainty after correction u_c owing to potential misattributions can be approximated by [24]

$$u_c \approx \frac{2N!}{(\frac{N+1}{2})!(\frac{N-1}{2})!}(1 - p_1)^{\frac{N+1}{2}}(f\tau_d)^{\frac{N-1}{2}}$$

with N the number of pumps in series and p_1 the average probability of all pumps to transfer exactly one electron per cycle. In the case of $N = 3$ as used here, this formula simplifies to $u_c \approx 6(1 - p_1)^2 f\tau_d$.

To evaluate the technical limits of this technique we assume a circuit with five serial pumps and increased detector bandwidth of $1/\tau_d \approx 50$ kHz obtainable by rf-SETs [32]. Assuming further a pumping frequency of $f = 1$ GHz and a pump error probability of $|1 - p_1| \approx 1 \times 10^{-6}$ as experimentally demonstrated [15] a very low relative uncertainty of $u_c < 10^{-8}$ seems feasible. This would enable a validated primary realization of the redefined electrical base unit ampere (A). Such device further

allows a direct closure of the quantum metrological triangle [33,34] to test the validity of electrical quantum metrology.

We thank N. Ubbelohde and A. Zorin for valuable discussion and acknowledge support in clean-room processing by P. Hinze. This work has been supported by the DFG and within the Joint Research Project "Quantum Ampere" (JRP SIB07) within the European Metrology Research Programme (EMRP). The EMRP is jointly funded by the EMRP participating countries within EURAMET and the European Union.

*Deceased.
†Corresponding author.
lukas.fricke@ptb.de
‡Corresponding author.
frank.hohls@ptb.de

[1] M. Planck, Ann. Phys. (Berlin) **306**, 69 (1900).
[2] B. D. Josephson, Phys. Lett. **1**, 251 (1962).
[3] K. v. Klitzing, G. Dorda, and M. Pepper, Phys. Rev. Lett. **45**, 494 (1980).
[4] CCEM, http://www.bipm.org/cc/CCEM/Allowed/26/CCEM-09-05.pdf (2009).
[5] BIPM, Resolution 1 of the 24th meeting of the CGPM, http://www.bipm.org/utils/common/pdf/24_CGPM_Resolutions.pdf (2011).
[6] L. J. Geerligs, V. F. Anderegg, P. A. M. Holweg, J. E. Mooij, H. Pothier, D. Esteve, C. Urbina, and M. H. Devoret, Phys. Rev. Lett. **64**, 2691 (1990).
[7] H. Pothier, P. Lafarge, C. Urbina, D. Esteve, and M. H. Devoret, Europhys. Lett. **17**, 249 (1992).
[8] M. W. Keller, J. M. Martinis, N. M. Zimmerman, and A. H. Steinbach, Appl. Phys. Lett. **69**, 1804 (1996).
[9] M. W. Keller, A. L. Eichenberger, J. M. Martinis, and N. M. Zimmerman, Science **285**, 1706 (1999).
[10] J. P. Pekola, J. J. Vartiainen, M. Möttönen, O.-P. Saira, M. Meschke, and D. V. Averin, Nat. Phys. **4**, 120 (2007).
[11] L. Nevou, V. Liverini, P. Friedli, F. Castellano, A. Bismuto, H. Sigg, F. Gramm, E. Müller, and J. Faist, Nat. Phys. **7**, 423 (2011).
[12] B. Roche, R.-P. Riwar, B. Voisin, E. Dupont-Ferrier, R. Wacquez, M. Vinet, M. Sanquer, J. Splettstoesser, and X. Jehl, Nat. Commun. **4**, 1581 (2013).
[13] M. D. Blumenthal, B. Kaestner, L. Li, S. Giblin, T. J. B. M. Janssen, M. Pepper, D. Anderson, G. Jones, and D. A. Ritchie, Nat. Phys. **3**, 343 (2007).
[14] B. Kaestner, V. Kashcheyevs, S. Amakawa, M. D. Blumenthal, L. Li, T. J. B. M. Janssen, G. Hein, K. Pierz, T. Weimann, U. Siegner, and H. W. Schumacher, Phys. Rev. B **77**, 153301 (2008).
[15] S. P. Giblin, M. Kataoka, J. D. Fletcher, P. See, T. J. B. M. Janssen, J. P. Griffiths, G. A. C. Jones, I. Farrer, and D. A. Ritchie, Nat. Commun. **3**, 930 (2012).
[16] J. P. Pekola, O.-P. Saira, V. F. Maisi, A. Kemppinen, M. Möttönen, Y. A. Pashkin, and D. V. Averin, Rev. Mod. Phys. **85**, 1421 (2013).
[17] D. V. Averin and K. K. Likharev, in *Mesoscopic Phenomena in Solids,* edited by B. L. Altshuler, P. A. Lee, and R. A. Webb (North Holland, Amsterdam, 1991), p. 173.
[18] N. M. Zimmerman, E. Hourdakis, Y. Ono, A. Fujiwara, and Y. Takahashi, J. Appl. Phys. **96**, 5254 (2004).
[19] V. Kashcheyevs and B. Kaestner, Phys. Rev. Lett. **104**, 186805 (2010).
[20] L. Fricke, M. Wulf, B. Kaestner, V. Kashcheyevs, J. Timoshenko, P. Nazarov, F. Hohls, P. Mirovsky, B. Mackrodt, R. Dolata, T. Weimann, K. Pierz, and H. W. Schumacher, Phys. Rev. Lett. **110**, 126803 (2013).
[21] N. Maire, F. Hohls, B. Kaestner, K. Pierz, H. W. Schumacher, and R. J. Haug, Appl. Phys. Lett. **92**, 082112 (2008).
[22] J. Bylander, T. Duty, and P. Delsing, Nature (London) **434**, 361 (2005).
[23] T. Fujisawa, T. Hayashi, R. Tomita, and Y. Hirayama, Science **312**, 1634 (2006).
[24] M. Wulf, Phys. Rev. B **87**, 035312 (2013).
[25] L. Fricke, F. Hohls, N. Ubbelohde, B. Kaestner, V. Kashcheyevs, C. Leicht, P. Mirovsky, K. Pierz, H. W. Schumacher, and R. J. Haug, Phys. Rev. B **83**, 193306 (2011).
[26] T. A. Fulton and G. J. Dolan, Phys. Rev. Lett. **59**, 109 (1987).
[27] L. S. Kuzmin, P. Delsing, T. Claeson, and K. K. Likharev, Phys. Rev. Lett. **62**, 2539 (1989).
[28] G. J. Dolan, Appl. Phys. Lett. **31**, 337 (1977).
[29] B. Kaestner, V. Kashcheyevs, G. Hein, K. Pierz, U. Siegner, and H. W. Schumacher, Appl. Phys. Lett. **92**, 192106 (2008).
[30] C. Leicht, B. Kaestner, V. Kashcheyevs, P. Mirovsky, T. Weimann, K. Pierz, and H. W. Schumacher, Physica (Amsterdam) **42E**, 911 (2010).
[31] See the Supplemental Material at http://link.aps.org/supplemental/10.1103/PhysRevLett.112.226803 for details about the measurement setup, the detector calibration as part of the counting algorithm, and the extraction of individual pump fidelities.
[32] R. J. Schoelkopf, P. Wahlgren, A. A. Kozhevnikov, P. Delsing, and D. E. Prober, Science **280**, 1238 (1998).
[33] K. K. Likharev and A. B. Zorin, J. Low Temp. Phys. **59**, 347 (1985).
[34] H. Scherer and B. Camarota, Meas. Sci. Technol. **23**, 124010 (2012).